IEEE Access
Multidisciplinary | Rapid Review | Open Access Journal

Received November 25, 2019, accepted December 6, 2019, date of publication December 13, 2019,
date of current version December 23, 2019.

Digital Object Identifier 10.1109/ACCESS.2019.2959204

Robust Line-Based Radial Distortion Estimation From a Single Image

LUWEI ZHANG[1,2,3], HONGBO SHANG[1,2], FANLU WU[1], RUI WANG[1,3], TAO SUN[1,3], AND JINGJIANG XIE[1,4]

[1]Changchun Institute of Optics, Fine Mechanics and Physics, Chinese Academy of Sciences, Changchun 130033, China
[2]Daheng College, University of Chinese Academy of Sciences, Beijing 100049, China
[3]State Key Laboratory of Laser Interaction with Matter, Changchun Institute of Optics, Fine Mechanics and Physics, Chinese Academy of Sciences, Changchun 130033, China
[4]Key Laboratory of Optical System Advanced Manufacturing Technology, Changchun Institute of Optics, Fine Mechanics and Physics, Chinese Academy of Sciences, Changchun 130033, China

Corresponding author: Hongbo Shang (shanghb@ciomp.ac.cn)

This work was supported in part by the State Key Laboratory of Laser Interaction with Matter under Grant SKLLIM1804, in part by the Jilin Scientific and Technological Development Program under Grant 20190302050G X, in part by the Youth Innovation Promotion Association of the Chinese Academy of Sciences under Grant 2016199, and in part by the National Natural Science Foundation of China under Grant 61705219.

ABSTRACT The pinhole model utilized in most computer vision algorithms becomes unfeasible because of lens distortion. Thus it is a must to compensate lens distortion to make the pinhole model available. In this paper, we propose a new robust line-based distortion estimation method to correct radial distortion. Our method works from a single image and is able to estimate the distortion center rather than assuming it is at the image center. Distortion parameters are estimated from parameters of circulars arcs, on the basis that straight lines are imaged as circular arcs under one-parameter division model. A new feature selection scheme by refining circular arcs is introduced to make the process of distortion estimation fully automatic and more robust. Moreover, a linear optimization algorithm is applied to calculating parameters in each selection run, making our feature selection scheme more efficient. Experiments on synthetic images and real images show that our method performs well in radial distortion estimation even with severely distorted images.

INDEX TERMS Distortion estimation, radial distortion, division model, feature selection, plumb-line.

I. INTRODUCTION

The pinhole model that straight lines in 3D world must project to straight lines in the image plane is the basis for most computer vision algorithms [1]. Due to the imperfection of lens and misalignment of optical elements, distortion is widely existed in optical systems, especially in fish-eye and wide angle lenses [2], [3]. The pinhole model is no longer available owing to mapping errors introduced by lens distortion. Thus it is a must to remove distortion accurately.

Among all distortion types, radial distortion is the most predominant one in today's cameras [4]–[6]. There are two main categories as to radial distortion estimation [7], that are multiple views method [5], [8]–[12], and single view method [13]–[17]. Multiple views method relies on known calibration objects [5], [8], sequence of images under camera motion or at different frames [9], [11], [12]. It is able to obtain distortion parameters and other camera parameters simultaneously. The main limitation of multiple views method is that it could not be applied to circumstances where a calibration pattern, a mobile camera and a video sequence are not available, for examples, dealing with images downloaded from website or real-time calibration of zoom cameras. On the contrast, the single view method does not need a special calibration object and is able to implement distortion estimation from a single image, which would be extremely useful for many applications, particularly those in human-made environments containing abundant lines [28]. One of the most promising single view method is the well-known plumb-line approach, which is on the basis of projective invariance that lines straight in 3D scenes will remain straight in 2D images. Many achievements based on plumb-line approach have been obtained in recent years [1], [15], [16], [25], [30]. Alemán-Flores *et al.* [18], [19], [32], [33], [35] studied on lens distortion correction by line rectification. Polynomial model as well as division model are utilized for distortion estimation. When dealing with severely distorted images, an extended Hough transform embedding the distortion

The associate editor coordinating the review of this manuscript and approving it for publication was Naveed Akhtar.

parameter is applied to detect longest distorted lines. Distortion parameters are optimized by minimizing the distance of the corrected line points to straight lines based on nonlinear algorithms. Bukhari and Dailey [6], [28] proposed an automatic distortion estimation method based on Fitzgibbon's division model [22]. They applied a two-step random sampling process to realize circle fitting and outlier elimination. Though their method works very well, sometimes it may be non-deterministic caused by RANSAC. To improve the robustness of distortion estimation, Benligiray and Topal [31] applied a sequential backward selection scheme to eliminate lines that come from non-collinear elements. Line orientation is taken as the error function, which is minimized using a nonlinear optimization algorithm. In their method, the distortion center is assumed to be at the image center, however, this assumption is not always true [20].

Our method proposed in this paper belongs to the plumb-line approach. Fitzgibbon's division model [22] is utilized as the distortion model because of its advantages in expressing large distortion with lower order [22]–[24], and the distortion center is estimated rather than assuming it is at the image center. Our estimator is partially similar to that of Wang *et al.* [25] and Wu *et al.* [7], on the principle that straight lines are modeled as circular arcs under one-parameter division model, and distortion parameters including distortion center can be obtained from the parameters of at least three circular arcs. There are two main advantages of our method over theirs include: (1) we improve the robustness and automatization of distortion estimation by introducing a new feature selection scheme. The effective features are selected automatically without human intervention and the results of distortion removal are robust. The feature selection scheme is conducted backwardly, making it more deterministic than RANSAC: each line is sequentially selected out of the lines group, and would be eliminated if its absence makes a minimum of the objective function. The selection run would be repeated until no further improvement in the objective function or there are only three lines left in the lines group. (2) No nonlinear optimization is needed in distortion model estimation, though it is usually used in other's work [7], [31]. Instead, a Linear Least Squares (**LLS**) optimization algorithm is applied to estimate distortion parameters when there are more than three lines. The efficiency of **LLS** algorithm outperforms the nonlinear algorithms significantly while with nearly the same accuracy, which would be shown in Section IV-A. Because the procedure of distortion parameters estimation is repeated in each selection run, the application of **LLS** algorithm would indeed save a lot of time for feature selection, thus making our feature selection scheme more efficient than the one used in [31].

The rest of the paper is organized as follows: In Section II, we introduce the proposed methodology for distortion estimation. Section III presents experimental results and detailed analyses. Section IV shows the comparison with other methods. Finally, we draw the conclusion in Section V.

II. METHODOLOGY

In this section, our robust distortion estimation method is explained in details. One-parameter division model is applied to distortion estimation, and under this distortion model, a straight line is imaged as a circular arc as described in Section II-A. Section II-B introduces how we detect lines and how we do robust circle fitting. Section II-C presents the **LLS** algorithm utilized to distortion parameters estimation with more than three lines. Furthermore, a feature selection scheme to improve the accuracy and robustness of distortion estimation is proposed in Section II-D.

A. DISTORTION MODELS AND DISTORTION OF A STRAIGHT LINE

In general, radial distortion is expressed in the following format [21]

$$\begin{pmatrix} x_u - x_0 \\ y_u - y_0 \end{pmatrix} = L\left(r_d\right) \begin{pmatrix} x_d - x_0 \\ y_d - y_0 \end{pmatrix}, \tag{1}$$

where (x_u, y_u) is the undistorted point, (x_d, y_d) is the distorted point, (x_0, y_0) is the distortion center, $L(r_d)$ represents the function which defines the shape of distortion and $r_d = \sqrt{(x_d - x_0)^2 + (y_d - y_0)^2}$. Different expression of $L(r_d)$ corresponds to different distortion model. Polynomial model and division model are two widely accepted distortion models among all radial distortion models.

Division model proposed by Fitzgibbon [22] is formulated as

$$L\left(r_d\right) = \frac{1}{1 + \lambda_1 r_d^2 + \lambda_2 r_d^4 + \lambda_3 r_d^6 + \cdots}. \tag{2}$$

The main advantage of division model over polynomial model is that it is able to express severe distortion at much lower order. In fact, for most cases, division model with one parameter would be sufficient [22]–[24].

In this paper, division model with single parameter is used, and defined as

$$L\left(r_d\right) = \frac{1}{1 + \lambda r_d^2} \tag{3}$$

Thus we obtain the mapping function from distorted points to rectified points as

$$\begin{cases} x_u - x_0 = \dfrac{x_d - x_0}{1 + \lambda r_d^2} \\ y_u - y_0 = \dfrac{y_d - y_0}{1 + \lambda r_d^2} \end{cases} \tag{4}$$

According to Wang *et al.* [25], a straight line can be imaged as a circular arc under one-parameter division model. Here, we define a straight line by

$$Ax_u + By_u + C = 0 \tag{5}$$

with the constraint $A^2 + B^2 > 0$. By substituting (4) to (5), we obtain the circle equation

$$(x_d - x_0)^2 + (y_d - y_0)^2 + \frac{A}{C\lambda}(x_d - x_0) + \frac{B}{C\lambda}(y_d - y_0) + \frac{1}{\lambda} = 0 \tag{6}$$

and it can be simplified as

$$x_d^2 + y_d^2 + Dx_d + Ey_d + F = 0 \tag{7}$$

where

$$\begin{aligned} D &= \frac{A}{C\lambda} - 2x_0, \\ E &= \frac{B}{C\lambda} - 2y_0, \\ F &= x_0^2 + y_0^2 - \frac{A}{C\lambda}x_0 - \frac{B}{C\lambda}y_0 + \frac{1}{\lambda}. \end{aligned} \tag{8}$$

B. CIRCLE FITTING ALGORITHM

Before circle fitting, curved lines detection is conducted. It starts with edge segments detection using Canny Operator, and then line segments detection from these edge segments. Line segments are detected by the straight line detector with a certain tolerance region, thus curved line segments can be detected. Afterwards, the detected curved line segments are further grouped according to their relative orientation and perpendicular distance. The detailed process for lines detection may be found in [29]. Furthermore, short features are reported to deteriorate performance in distortion estimation, hence they are eliminated [31]. According to our experience, a threshold on the length of the extracted lines is set one fifteenth the image width, and is used systematically in the following experiments.

To accurately fit a curved line to a circle is to minimize the sum of squared distances from data points to the fitting circle. For n data points $(x_i, y_i)_{i=1\ldots n}$, the error function can be expressed as

$$\varepsilon = \sum_{i=1}^{n} d_i^2, \tag{9}$$

where d_i represents the Euclidean distance from the data point (x_i, y_i) to the fitting circle, and is defined by

$$d_i = \sqrt{(x_i - a)^2 + (y_i - b)^2} - R, \tag{10}$$

where (a, b) is the center and R is the radius of the fitting circle.

To robustly find the minimum of (9), We choose Levenberg-Marquardt (**LM**) iterative nonlinear algorithm to realize circle fitting. A good initial guess is necessary for convergence to the optimal minimum and reduction of iteration times. Here, Taubin Fit is adopted as an algebraic fit method to provide an initial guess to **LM** circle fitting. Details about **LM** Fit and Taubin Fit as well as comparisons between different circle fitting methods please see [26]–[28].

C. DISTORTION ESTIMATION WITH MULTIPLE LINES USING LLS ALGORITHM

Wang *et al.* [25] show it is possible to estimate distortion center (x_0, y_0) as well as distortion coefficient λ with three circular arcs extracted from the distorted image. Here, we briefly review their algorithm in dealing with three circular arcs and then introduce our algorithm for distortion estimation with multiple lines (more than three lines).

Based on the definition of D, E, and F as shown in (8), we obtain

$$\frac{1}{\lambda} = x_0^2 + y_0^2 + Dx_0 + Ey_0 + F. \tag{11}$$

Then we can calculate the distortion center (x_0, y_0) as long as we determine three groups of parameters $(D_i, E_i, F_i)_{i=1,2,3}$, which are obtained through the circle fitting algorithm presented in Section II-B. The distortion center (x_0, y_0) is obtained by solving the following linear equations

$$\begin{cases} (D_1 - D_2)\, x_0 + (E_1 - E_2)\, y_0 + (F_1 - F_2) = 0 \\ (D_1 - D_3)\, x_0 + (E_1 - E_3)\, y_0 + (F_1 - F_3) = 0 \end{cases} \tag{12}$$

After the distortion center is determined, the distortion coefficient λ is calculated by (11).

To achieve higher accuracy, always more than three circular arcs are utilized for distortion parameters estimation. For cases there are more than three circular arcs, we calculate the distortion parameters using the following **LLS** algorithm. We modify (12) to

$$\left(D_i - D_j\right) x_0 + \left(E_i - E_j\right) y_0 = F_j - F_i (i \neq j). \tag{13}$$

Then we have

$$MX = N, \tag{14}$$

where $X = (x_0, y_0)^T$, $N = (F_j - F_i)_{i \neq j}$, $M = (D_i - D_j, E_i - E_j)_{i \neq j}$, and M is a non-square matrix. Then the distortion center (x_0, y_0) and the distortion coefficient λ can be obtained respectively by (15) and (16)

$$(x_0, y_0)^T = \left(M^T M\right)^{-1} M^T N \tag{15}$$

$$\lambda = \frac{1}{x_0^2 + y_0^2 + \overline{D}x_0 + \overline{E}y_0 + \overline{F}}, \tag{16}$$

where $\overline{D}, \overline{E}$, and $\overline{F}$ are the mean value of D_i, E_i, and F_i. Although this algorithm is usually applied with more than three lines from a single image, it is also able to handle distortion parameters estimation for circumstances with fewer lines by taking more images with the same camera or assuming the distortion center is at the image center when more images are not available.

LLS algorithm is non-iterative, thus it does not need initial input and is more computing efficient. Comparisons between **LLS** algorithm and **LM** algorithm used in [7] in terms of results accuracy and computing time are shown in Section IV-A.

D. ROBUST DISTORTION ESTIMATION WITH CIRCULAR ARCS REFINING

This section is of great importance to the robustness of our distortion estimation method. Since distortion parameters are obtained from circular arcs parameters according to (15) and (16), the robustness and accuracy of distortion parameters

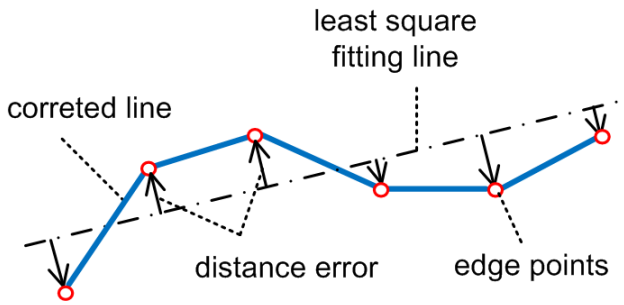

FIGURE 1. The distance error of one line is the mean of square distances from all edge points on the corrected line to the least square fitting line corresponding to these edge points.

estimation is highly relevant to the validity of extracted circular arcs.

RANSAC is widely used for the selection of effective features [28]–[30]. However, sometimes it may fail to be deterministic especially when there are large numbers of features. Benligiray and Topal [31] proposed a sequential backward selection scheme to make feature selection more robust. In each iteration loop, they utilized line orientation as the error function, and conducted nonlinear iterative optimization to minimize the error function. Inspired by their method but differently, we propose a feature selection scheme based on distance error to refine circular arcs sequentially, considering that distance error is less sensitive to step points existed in lines extracted from low resolution images. Besides, in each selection run, we recalculate distortion parameters by **LLS** algorithm rather than other nonlinear iterative algorithms, making our feature selection scheme more efficient than Benligiray and Topal's [31].

An objective function based on distance error is adopted as a metric to the straightness of the rectified lines. The distance error of one rectified line (see Fig. 1) is defined by

$$\varepsilon_i = \frac{1}{n_i}\sum_{j=1}^{n_i} d_{i,j}^2, \tag{17}$$

where $d_{i,j}$ is the distance from the jth edge point on the ith rectified line to the least square fitting line corresponding to these edge points. Given N corrected lines corresponding to N distorted lines, the objective function is defined by the mean distance error of all N corrected lines as

$$\Phi = \frac{1}{N}\sum_{i=1}^{N} \varepsilon_i. \tag{18}$$

Here, N refers to all detected long lines before feature selection, rather than the lines retained in each selection run. The advantage of this definition for objective function is that we are able to avoid a local minimum only for the remaining lines, on the basis that majority of the detected long lines are expected to be real lines in 3D world.

We refine extracted circular arcs in two folds: (1) Is it a true arc? (2) Is it a good arc that can provide better performance in distortion estimation? If true arcs with good quality

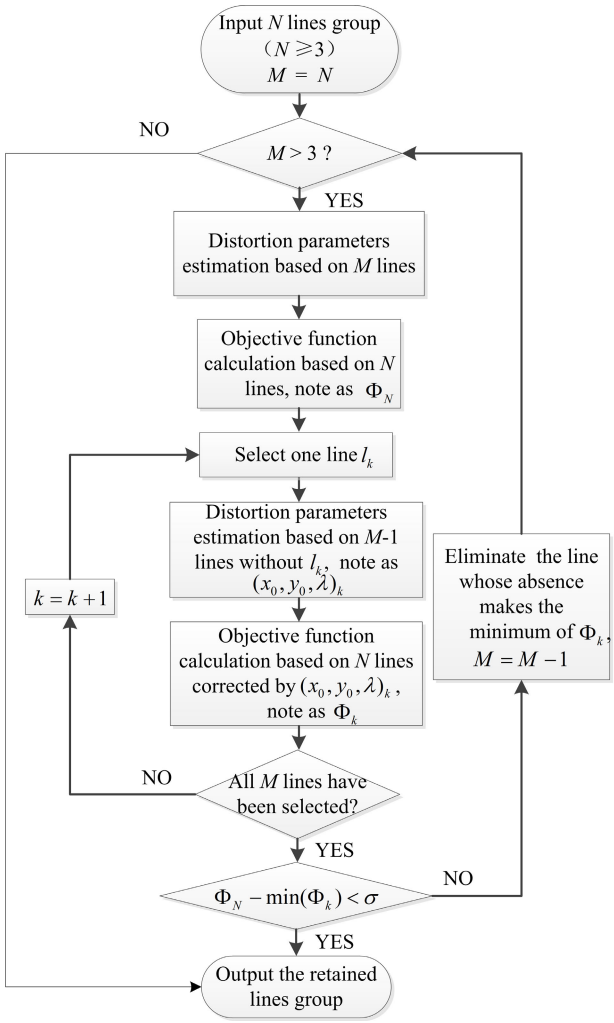

FIGURE 2. Flow chart of proposed circular arcs refining scheme.

(efficient distortion, low noise, *etc.*) are selected and utilized to distortion estimation, the objective function defined by (18) will decrease. It is realized by removing unvalid arcs from the lines group, and the whole process is conducted backwardly: each line is initially excluded from the lines group one by one, and would be indeed eliminated if its absence makes a minimum of the objective function defined in (18). The selection run would be repeated until the objective function is not improved with elimination of any line or there are only three lines left in the lines group. We have to mention that our proposed circular arcs refining scheme is only conducted when there are more than three lines as our method needs at least three lines for distortion parameters estimation. Fig. 2 represents the whole process of this scheme. Firstly, we estimate the distortion parameters with all M lines and calculate the objective function. Then we select one line out of the M lines group, re-estimate the distortion parameters with the remaining M-1 lines and recalculate the objective function. We repeat the above procedures until all lines have been selected sequentially. Then the line whose absence makes the minimum objective function is eliminated

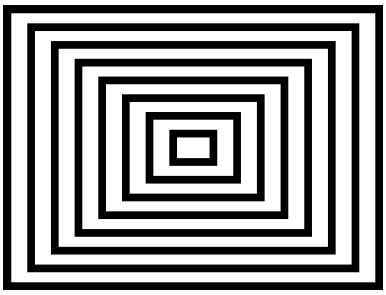

FIGURE 3. Source image.

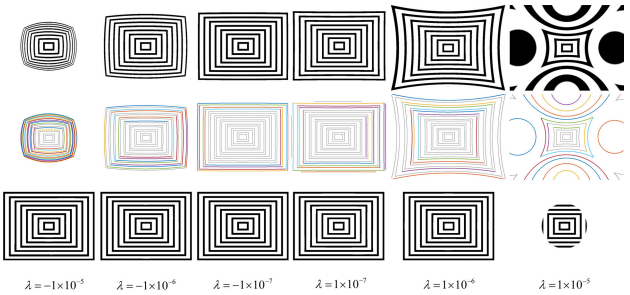

FIGURE 4. Distortion correction of synthetic images with different distortion coefficients. ***First row***: distorted images. ***Second row***: corresponding refined circular arcs utilized to distortion estimation. ***Third row***: corresponding undistorted images using parameters calculated by our method.

from the lines group. Here we set a threshold of $\sigma = 0.01$ for the reduction of objective function to judge whether the line is really needed to be eliminated. It means that only if the objective function diminishes more than 0.01 when the line is excluded from the lines group, the line is indeed eliminated. After a line is actually removed from the lines group, we repeat the above procedures with the remaining lines. The iteration stops if there is no further improvement in the objective function with exclusion of any line or there are only three lines left in the lines group. Then the optimal distortion parameters are obtained with the remaining lines and thus the distorted image is corrected. It is worth mentioning that **LLS** algorithm is applied to estimate distortion parameters in each selection run when there are more than three lines, which would improve the efficiency of our feature selection scheme significantly.

III. EXPERIMENTS AND RESULTS

In this section, to evaluate our proposed method for distortion estimation in a quantitative and extensive way, we would firstly conduct experiments on a series of synthetic images from the same source image as shown in Fig. 3. The experiments are carried out in three series: varying distortion coefficient, varying distortion center and under different noise levels. Thus we would demonstrate our method's ability in severe and small distortion removal, distortion center estimation and distortion correction for noisy images. Secondly, we would conduct experiments on real images for qualitative evaluation. A detailed example of one real image is presented to illustrate how our method works and show the improvement with our circular arcs refining scheme. Afterwards, more challenging real images with different scenes are utilized to testify the performance of our method in removing most visible distortion.

A. SYNTHETIC IMAGES

The size of the source image shown in Fig. 3 is 640 × 480. The synthetic images utilized in following experiments are all from the same source image. To quantitatively evaluate the performance of our proposed method, *Dis_center* and *Rel_lambda* are applied to evaluate the deviation of estimated distortion parameters from true data. *Dis_center* is the Euclidean distance between $(x_0, y_0)_{true}$ and $(x_0, y_0)_{estimate}$. *Rel_lambda* is the absolute relative error of λ defined by $|(\lambda_{\text{estimate}} - \lambda_{\text{true}})/\lambda_{\text{true}}|$. Besides, Root Mean-Squared Error (RMSE) and Peak Signal-to-Noise Ratio (PSNR) are also adopted in this part to evaluate the performance of our method in reconstructing the source image.

1) VARYING DISTORTION COEFFICIENT

In the 1st series, we only change the distortion coefficient λ of each synthetic image while keeping the distortion center unchanged. The distortion center is fixed at the image center (320, 240), and the distortion coefficient λ varies from negative to positive. For negative λ, the synthetic image is smaller than the source image. For positive λ, the synthetic image is larger than the source image. For severe positive distortion of $\lambda = 1 \times 10^{-5}$, the distorted image is too large to display, thus only its central part with image size of 800 × 600 is shown. For each run, we refine circular arcs by our sequential selection scheme, and estimate distortion parameters (x_0, y_0, λ) with remaining circular arcs. The synthetic images under different distortion levels, corresponding refined circular arcs and corresponding corrected images are shown in Fig. 4. For $\lambda = 1 \times 10^{-5}$, only points with $r_u^2 \leq 1/4\lambda$ are mapped resulting in a centered circular valid region in the undistorted image.

The results of *Dis_center*, *Rel_lambda*, RMSE and PSNR are shown in Fig. 5. For $\lambda = 1 \times 10^{-5}$, RMSE and PSNR are only measured over the circular valid region shown in Fig. 4. In addition, RMSE and PSNR calculated from true data corrected images are also displayed in Fig. 5(c) and Fig. 5(d) respectively for comparison. Theoretically, RMSE would be zero and PSNR would be infinity if the distorted image is corrected with the ground truth data. However, due to errors introduced by various calculations such as interpolation, RMSE and PSNR of true data corrected images are not able to reach the theoretical values. Hence, in our experiments, results of true data corrected images are displayed as the ideal values. From Fig. 5, we observe that our method works quite well in distortion correction. The estimated distortion parameters are very close to the true data, as both *Dis_center* and *Rel_lambda* are very small with varying lambda. The maximum of *Dis_center* and *Rel_lambda* exist at distortion level of $\lambda = 1 \times 10^{-7}$, with values of less than 2.7000 pixels

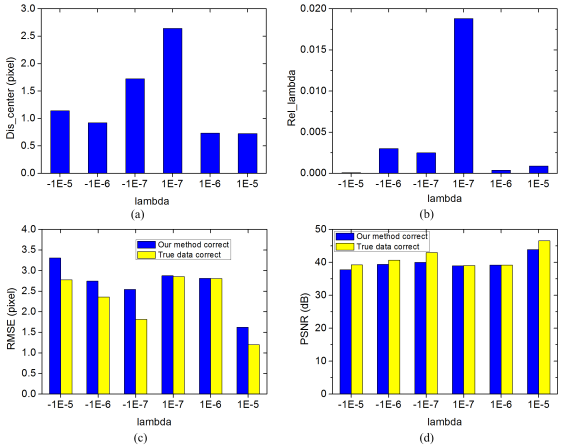

FIGURE 5. Results of distortion estimation with varying lambda. (a) *Dis_center*. (b) *Rel_lambda*. (c) RMSE of our method corrected images and true data corrected images. (d) PSNR of our method corrected images and true data corrected images.

and less than 0.0200 respectively. The relatively poor results with small distortion is because in low distortion levels, small deviations in estimated distortion parameters would create a relatively large error. In fact, though there is a slight drop in performance under small distortion levels, the results are still of high accuracy since RMSE and PSNR are very close to the ideal values as shown in Fig. 5(c) and Fig. 5(d). These experimental results demonstrate our method's ability in distortion correction of images with severe distortion as well as small distortion.

2) VARYING DISTORTION CENTER

In the 2nd series, we fix the distortion level at $\lambda = -1 \times 10^{-6}$ and vary the distortion center. There are 62 extracted arcs for each synthetic image, and then distortion estimation is conducted with circular arcs refining. The experimental results are listed in Table 1. From Table 1, we can observe that our method has good performance in distortion removal for images whose distortion center is not at the image center, and the performance has little to do with the offset between the distortion center and the image center. RMSE under different distortion center is less than 3.3000 pixels, and PSNR is more than 37.9000 *dB*. These results are quite close to the results calculated from true data corrected images.

3) UNDER DIFFERENT NOISE LEVELS

In the 3rd series, we append Gaussian noise with 0 mean and standard deviation ranging from 0.1 to 1 pixel, which is considered to be normal level noise [36], to the extracted circular arcs from the synthetic image with $\lambda = 1 \times 10^{-6}$ and $(x_0, y_0) =$| (320, 240).The results of RMSE and PSNR as Gaussian noise varies from 0.1 to 1 pixel are displayed in Fig. 6, and the values are the mean of 100 trials. From Fig. 6(a), we can see that RMSE increases with the noise level whether we refine circular arcs or not. In fact, with circular arcs refining, RMSE increases very slowly especially when the noise level is less than 0.7 pixel. RMSE is less than

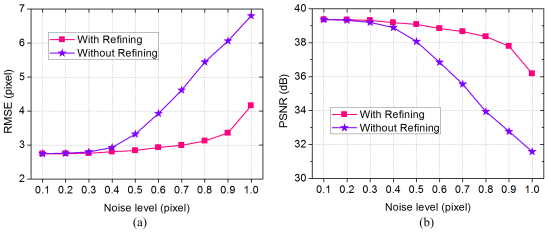

FIGURE 6. Results under different noise level. (a) RMSE. (b) PSNR.

3.0000 pixels in noise level of 0.7 pixel and it is 4.1609 pixels in noise level of 1 pixel. The results are quite acceptable for most practical circumstances. However, without circular arcs refining, RMSE increases much faster with noise level. RMSE comes to 4.6155 pixels in noise level of 0.7 pixel and 6.8016 pixels in noise level of 1 pixel, which are more than 50% larger than that calculated by our method with circular arcs refining. Fig. 6(b) shows that PSNR decreases with the noise level. The value of PSNR is higher, the quality of reconstructed image is better. Generally, when PSNR is more than 35.0000 *dB*, the quality of reconstructed image is considered to be satisfactory. With circular arcs refining, the results of PSNR are all higher than 35.0000 *dB* under different level of noise. With 1 pixel noise, PSNR is 36.1799 *dB*, while the value is deteriorated to 31.5832 *dB* without circular arcs refining. Through comparison, we can see that our method is very robust in distortion removal of images with normal level noise.

B. REAL IMAGES

Here, we present a qualitative evaluation of our method's ability in distortion removal of real images with significant distortion. Fig. 7 shows results of one real image from Santana-Cedrés *et al.* [33]. The image size is 1424 × 2144. The distorted image is shown in Fig. 7(a), and the corresponding detected edges obtained by applying Canny Operator is shown in Fig. 7(b). Then lines detection is conducted, and according to the threshold set for the length of lines as mentioned in Section II-B, only 52 lines longer than 100 pixels are retained in the lines group as shown in Fig. 7(c). Then circular arcs refining is conducted according to Section II-D and after applying the refinement process, 39 lines are finally retained, as shown in Fig. 7(d), to obtain optimal distortion parameters. For comparison, image corrected without circular arcs refining (using 52 long lines in Fig. 7(c)) and image corrected with circular arcs refining (using 39 lines in Fig. 7(d)) are shown in Fig. 7(e) and Fig. 7(f), respectively. Fig. 7(e) and Fig. 7(f) are with the same image size, and not scaled or translated. We can observe that Fig. 7(f) outperforms Fig. 7(e) distinctly in visual quality, and this comparison shows that the performance of distortion estimation and removal has been greatly improved with our feature selection scheme.

Since our distortion estimation from a single image is based on the lines existed in the image, it would be very useful for many applications, especially those in human-made environments containing abundant lines. Though human-made

TABLE 1. Distortion estimation results of synthetic images with different distortion center. The unit of RMSE is pixel and the unit of PSNR is *dB* in the table.

$(x_0, y_0)_{true}$	Estimated by our method							True data Correct	
	refined circular arcs	$(x_0, y_0)_{estimate}$	Dis_center	$\lambda_{estimate}$	Rel_lambda	RMSE	PSNR	RMSE	PSNR
(240, 320)	41	(240.3716, 319.5285)	0.6003	-9.9422×10^{-7}	5.8000×10^{-3}	2.8438	39.0527	2.8111	39.1532
(260, 300)	35	(263.3810, 298.6390)	3.6447	-1.0011×10^{-6}	1.1000×10^{-3}	3.0140	38.5479	2.8276	39.1024
(280, 280)	43	(281.5717, 278.9583)	1.8856	-9.9829×10^{-7}	1.7000×10^{-3}	2.7904	39.2176	2.7378	39.3827
(300, 260)	33	(296.3730, 258.9285)	3.7820	-1.0034×10^{-6}	3.4000×10^{-3}	3.2417	37.9153	2.8167	39.1359
(340, 220)	39	(337.3410, 219.0150)	2.8356	-1.0019×10^{-6}	1.9000×10^{-3}	2.8932	38.9033	2.7965	39.1986
(360, 200)	42	(358.4634, 198.6244)	2.0624	-9.9276×10^{-7}	7.2000×10^{-3}	2.8577	39.0105	2.7804	39.2487
(380, 180)	39	(380.7630, 178.7657)	1.4511	-1.0002×10^{-6}	2.4940×10^{-4}	2.7917	39.2134	2.7901	39.2185
(400, 160)	38	(397.5426, 158.6079)	2.8243	-9.9491×10^{-7}	5.1000×10^{-3}	2.9626	38.6972	2.8288	39.0988

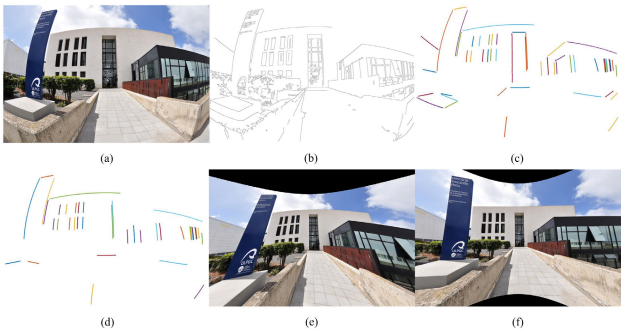

FIGURE 7. Results of one real image from Santana-Cedrés *et al.* [33]. (a) Distorted image. (b) Detected edges. (c) Identified long lines. (d) Remaining lines after circular arcs refining. (e) Undistorted image without circular arcs refining (using identified long lines in Fig. 7(c)). (f) Undistorted image with circular arcs refining (using remaining lines in Fig. 7(d)). (The different colors of lines are set for a clearer display, not representing the belonging to one or another line.)

FIGURE 8. Correction of some challenging real images from previous papers on distortion estimation [33], [34]. Column 1 and column 3 are original distorted images. Column 2 and column 4 are corresponding undistorted images using parameters estimated by our proposed method.

environments usually follow the Manhattan World Assumption, our method doesn't use this constraint, instead only use the constraint that straight lines in the 3D world must be straight lines in 2D image if distortion is compensated. As long as there are several real lines in the image, our method is available. For cases there are a few curves in 3D world mistaken for straight lines after lines detection, the wrong lines would be further eliminated with our circular arcs refining scheme as the objective function usually diminishes with the absence of the wrong lines. Fig. 8 presents experiments on a set of challenging real images with different scenes from previous papers on distortion estimation [33], [34]. As to the last real image, there are only a few short lines in the scene, thus the distortion center is assumed to be at the image center. The results shown in Fig. 8 demonstrate that our method is able to remove most of the visible distortion for real images containing several real lines. It is also worth mentioning that for worst cases that wrong lines are predominant in the images, it is better to refine circular arcs with human intervention to obtain better performance of distortion removal.

IV. COMPARE WITH OTHER METHODS

A. COMPARE LLS ALGORITHM WITH LM ALGORITHM

In Wu *et al.*'s [7] method, **LM** iterative nonlinear least squares algorithm is applied to calculate distortion parameters with more than three circular arcs. However, in our method, **LLS** algorithm is utilized. A comparison between **LLS** algorithm and **LM** algorithm in terms of computing accuracy and efficiency is conducted below. The circular arcs utilized in the following experiments are part of those extracted from a synthetic image made from the source image shown in Fig. 3 with $\lambda = 1\times10^{-6}$ and $(x_0, y_0) = (320, 240)$. The same circular arcs are utilized to calculate distortion parameters for both algorithms (**LLS** and **LM**). Here, **LLS** algorithm is conducted without the need of initial estimation, while **LM** algorithm is conducted with initial input of $\lambda = -1.1175\times10^{-6}$ and $(x_0, y_0) = (353.7563, 216.3052)$. The initial value provided to **LM** algorithm is obtained from three marginal circular arcs according to (11) and (12). The results are shown in Table 2, and running time listed in this table is the mean computing time of 100 trials for distortion parameters calculation by solving (11) and (13) with **LLS** and **LM** algorithm. It can be seen that distortion parameters obtained by **LLS** algorithm is very close to those obtained by

TABLE 2. The comparison between LLS algorithm and LM algorithm.

Number of lines	Algorithm	$(x_0, y_0)_{estimate}$	$\lambda_{estimate}$	*Dis_center*	*Rel_lambda*	Running time
28	**LLS**	(320.6203, 238.3567)	-1.0064×10^{-6}	1.7564	6.40×10^{-3}	0.006s
	LM	(320.6203, 238.3567)	-1.0064×10^{-6}	1.7564	6.40×10^{-3}	1.671s
24	**LLS**	(320.5978, 238.4246)	-1.0002×10^{-6}	1.6850	-2.40×10^{-4}	0.006s
	LM	(320.5978, 238.4246)	-1.0002×10^{-6}	1.6850	-2.40×10^{-4}	1.639s
20	**LLS**	(320.6032, 238.8090)	-9.9295×10^{-7}	1.3350	7.10×10^{-3}	0.006s
	LM	(320.6032, 238.8090)	-9.9295×10^{-7}	1.3350	7.10×10^{-3}	1.432s
16	**LLS**	(320.6502, 240.5879)	-9.9900×10^{-7}	0.8766	1.00×10^{-3}	0.005s
	LM	(320.6502, 240.5879)	-9.9900×10^{-7}	0.8766	1.00×10^{-3}	1.286s
12	**LLS**	(320.6599, 239.9361)	-1.0005×10^{-6}	0.6629	-4.94×10^{-4}	0.005s
	LM	(320.6599, 239.9361)	-1.0005×10^{-6}	0.6629	-4.94×10^{-4}	1.240s

TABLE 3. Comparison with Santana-Cedrés *et al.* [33]. The unit of RMSE is pixel and the unit of PSNR is *dB* in the table.

(x_0, y_0)	Method		Estimated data correct		True data correct	
			RMSE	PSNR	RMSE	PSNR
(320, 240)	Santana-Cedrés *et al.*	division model	3.6589	36.8638	2.3552	40.6902
		polynomial model	3.7938	36.5494		
	Our method		2.7448	39.3607		
(300, 260)	Santana-Cedrés *et al.*	division model	6.0324	32.5210	2.8167	39.1359
		polynomial model	5.9050	32.7064		
	Our method		3.2417	37.9153		

LM algorithm (their values are the same under the effective digits listed in Table 2), including both distortion center and distortion coefficient. This is true when we apply different number of circular arcs to distortion estimation. It means that our **LLS** algorithm can achieve nearly the same accuracy as **LM** algorithm in distortion parameters calculation. But our **LLS** algorithm is non-iterative and thus more computationally efficient than **LM** algorithm. In our experiments, **LLS** algorithm is more than two orders of magnitude faster than **LM** algorithm under the same working conditions as shown in Table 2.

B. COMPARE OUR METHOD WITH SANTANA-CEDRÉS et al.'s method

Finally, we compare our method with Santana-Cedrés *et al.*'s [33] method. They have conducted continuous study on radial distortion estimation, and published several related articles [18], [19], [32], [33], [35]. Moreover, they have provided an online demo for their automatic distortion correction method, which is available to anyone interested in their study. In the latest version of their demo, they applied an improved Hough transform to detect distorted lines, and then used nonlinear iterative optimization to estimate distortion model. In their demo interface, the users could choose two-parameter division model or two-parameter polynomial model as the distortion model and whether to handle distortion center estimation. For a fair comparison with our method, the option for optimization of the center of the lens distortion model is chosen. The comparison between our method and Santana-Cedrés *et al.*'s method are firstly carried out with synthetic images. Two synthetic images, which are with the same image size of 640 $\times$ 480 and the same distortion level of $\lambda = -1 \times 10^{-6}$, while with different distortion center, are used for quantitative comparison. The corrected images obtained from Santana-Cedrés *et al.* are scaled and translated properly to match the original undistorted image best. The experimental results are shown in Table 3. We can observe that in Santana-Cedrés *et al.*'s method two-parameter division model and two-parameter polynomial model have similar performance. Their method works well when the distortion center is at the image center (320,240), but its performance is not satisfactory when the center of distortion deviates from the center of the image though distortion center estimation is indeed conducted. Conversely, the results of our method are very close to the results obtained from true data corrected image regardless of whether the distortion center is at the image center. For distortion center of (320, 240) and (300, 260), the PSNR obtained by our method are 6.77 % and 15.93 % higher than the values of Santana-Cedrés *et al.*'s method, respectively. Secondly, two real images from [33], [34] are utilized for further comparison and the results are shown in Fig. 9. In Fig. 9(a), both two methods succeed in removing most of the distortion. However, in Fig. 9(b), the visual quality of undistorted image obtained by Santana-Cedrés *et al.*'s method is evidently worse than the one obtained by our method, for there is obvious residual distortion in their undistorted image, which may be easily seen in the right marginal region. The possible reason may be the actual distortion center of Fig. 9(b) is a little far from the image center, and Santana-Cedrés *et al.*'s method could not properly handle the distortion center estimation, which is in accordance with the results of experiments on synthetic images. Therefore, it is demonstrated by the above experiments that our method outperforms Santana-Cedrés *et al.*'s method in distortion estimation especially when the distortion center is not at the center of the image.

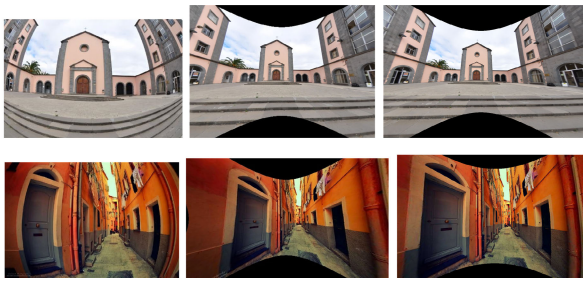

FIGURE 9. Distortion estimation results of our method and Santana-Cedrés *et al.*'s [33] method with real images from [33], [34]. Column 1 are original distorted images. Column 2 are undistorted images obtained by our method. Column 3 are undistorted images obtained by Santana-Cedrés *et al.*'s method with two-parameter division model.

V. CONCLUSION

In this paper, a robust line-based method is proposed for distortion estimation. It does not require a special calibration pattern, and is able to implement distortion correction from a single image as long as there are several lines, which is accessible for most human-made environments. Experiments on abundant synthetic images and real images have demonstrated our method's ability in estimating distortion parameters with high robustness and accuracy. The main contributions including novelties of this paper are: 1) a new distance-error based circular arcs refining scheme is proposed to make our feature selection fully automatic and more robust, and has been proven to significantly improve the performance of distortion estimation; 2) **LLS** linear algorithm is introduced to distortion parameters calculation in each feature selection run, which is much faster than **LM** nonlinear algorithm with nearly the same accuracy, thus making our feature selection scheme more efficient; 3) robust distortion center estimation is implemented by our method and it has been manifested that our method outperforms a publicly accessible method in distortion estimation of images especially those whose distortion center is not at the image center.

REFERENCES

[1] F. Devernay and O. Faugeras, "Straight lines have to be straight: Automatic calibration and removal of distortion from scenes of structured environments," *Mach. Vis. Appl.*, vol. 13, no. 1, pp. 14–24, 2001, doi: 10.1007/PL00013269.

[2] M. Friel, C. Hughes, P. Denny, E. Jones, and M. Glavin, "Automatic calibration of fish-eye cameras from automotive video sequences," *IET Intell. Transp. Syst.*, vol. 4, no. 2, pp. 136–148, 2010, doi: 10.1049/iet-its.2009.0052.

[3] X.-X. Zhang *et al.*, "Wide-field auroral imager onboard the Fengyun satellite," *Light-Sci. Appl.*, vol. 8, May 2019, Art. no. 47, doi: 10.1038/s41377-019-0157-7.

[4] Z. Kukelova and T. Pajdla, "A minimal solution to radial distortion autocalibration," *IEEE Trans. Pattern Anal. Mach. Intell.*, vol. 33, no. 12, pp. 2410–2422, Dec. 2011, doi: 10.1109/TPAMI.2011.86.

[5] Z. Y. Zhang, "A flexible new technique for camera calibration," *IEEE Trans. Pattern Anal. Mach. Intell.*, vol. 22, no. 11, pp. 1330–1334, Nov. 2000, doi: 10.1109/34.888718.

[6] F. Bukhari and M. N. Dailey, "Robust radial distortion from a single image," in *Proc. Int. Symp. Vis. Comput.*, Berlin, Germany, 2010, pp. 11–20, doi: 10.1007/978-3-642-17274-8_2.

[7] F. L. Wu, H. Wei, and X. J. Wang, "Correction of image radial distortion based on division model," *Opt. Eng.*, vol. 56, no. 1, 2017, Art. no. 013108, doi: 10.1117/1.OE.56.1.013108.

[8] R. Tsai, "A versatile camera calibration technique for high-accuracy 3D machine vision metrology using off-the-shelf TV cameras and lenses," *IEEE Trans. Robot. Autom.*, vol. RA-3, no. 4, pp. 323–344, Aug. 1987, doi: 10.1109/JRA.1987.1087109.

[9] S. Ramalingam, P. Sturm, and S. K. Lodha, "Generic self-calibration of central cameras," *Comput. Vis. Image Understand.*, vol. 114, no. 2, pp. 210–219, 2010, doi: 10.1016/j.cviu.2009.07.007.

[10] X. Du, H. Li, and Y. Zhu, "Camera lens radial distortion correction using two-view projective invariants," *Opt. Lett.*, vol. 36, no. 24, pp. 4734–4736, 2011, doi: 10.1364/OL.36.004734.

[11] B. Micusik and T. Pajdla, "Structure from motion with wide circular field of view cameras," *IEEE Trans. Pattern Anal. Mach. Intell.*, vol. 28, no. 7, pp. 1135–1149, Jul. 2006, doi: 10.1109/TPAMI.2006.151.

[12] Z. Tang, Y.-S. Lin, K.-H. Lee, J.-N. Hwang, and J.-H. Chuang, "ESTHER: Joint camera self-calibration and automatic radial distortion correction from tracking of walking humans," *IEEE Access*, vol. 7, pp. 10754–10766, 2019, doi: 10.1109/ACCESS.2019.2891224.

[13] S. H. Jiang, D. H. Cao, Y. B. Wu, S. Zhu, and P. Hu, "Efficient line based lens distortion correction for complete distortion with vanishing point constraint," *Appl. Opt.*, vol. 54, no. 14, pp. 4432–4438, 2015, doi: 10.1364/AO.54.004432.

[14] M. Lee, H. Kim, and J. Paik, "Correction of barrel distortion in fisheye lens images using image-based estimation of distortion parameters," *IEEE Access*, vol. 7, pp. 45723–45733, 2019, doi: 10.1109/ACCESS.2019.2908451.

[15] R. Strand and E. Hayman, "Correcting radial distortion by circle fitting," in *Proc. Brit. Mach. Vis. Conf. (BMVC)*, 2005, doi: 10.5244/C.19.9.

[16] E. Rosten and R. Loveland, "Camera distortion self-calibration using the plumb-line constraint and minimal Hough entropy," *Mach. Vis. Appl.*, vol. 22, no. 1, pp. 77–85, 2011, doi: 10.1007/s00138-009-0196-9.

[17] F. Wu, H. Guan, D. Yan, Z. Wang, D. Wang, and Q. Meng, "Precise geometric correction and robust mosaicking for airborne lightweight optical butting infrared imaging system," *IEEE Access*, vol. 7, pp. 93569–93579, 2019, doi: 10.1109/ACCESS.2019.2928380.

[18] M. Alemán-Flores, L. Alvarez, L. Gomez, and D. Santana-Cedrés, "Line detection in images showing significant lens distortion and application to distortion correction," *Pattern Recognit. Lett.*, vol. 36, pp. 261–271, Jan. 2014, doi: 10.1016/j.patrec.2013.06.020.

[19] M. Alemán-Flores, L. Alvarez, L. Gomez, and D. Santana-Cedrés, "Wide-angle lens distortion correction using division models," in *Proc. Iberoamer. Congr. Pattern Recognit.*, Berlin, Germany, 2013, pp. 415–422, doi: 10.1007/978-3-642-41822-8_52.

[20] R. Hartley and S. B. Kang, "Parameter-free radial distortion correction with center of distortion estimation," *IEEE Trans. Pattern Anal. Mach. Intell.*, vol. 29, no. 8, pp. 1309–1321, Aug. 2007, doi: 10.1109/TPAMI.2007.1147.

[21] D. C. Brown, "Close-range camera calibration," *Photogramm. Eng.*, vol. 37, no. 8, pp. 855–866, 1971.

[22] A. W. Fitzgibbon, "Simultaneous linear estimation of multiple view geometry and lens distortion," in *Proc. IEEE Comput. Soc. Conf. Comput. Vis. Pattern Recognit. (CVPR)*, Kauai, HI, USA, Dec. 2001, pp. 125–132, doi: 10.1109/CVPR.2001.990465.

[23] D. Claus and A. W. Fitzgibbon, "A rational function lens distortion model for general cameras," in *Proc. IEEE Comput. Soc. Conf. Comput. Vis. Pattern Recognit. (CVPR)*, San Diego, CA, USA, Jun. 2005, pp. 213–219, doi: 10.1109/CVPR.2005.43.

[24] C. Ricolfe-Viala and A. Sanchez-Salmeron, "Lens distortion models evaluation," *Appl. Opt.*, vol. 49, no. 30, pp. 5914–5928, 2010, doi: 10.1364/AO.49.005914.

[25] A. Wang, T. Qiu, and L. Shao, "A simple method of radial distortion correction with centre of distortion estimation," *J. Math. Imag. Vis.*, vol. 35, no. 3, pp. 165–172, 2009, doi: 10.1007/s10851-009-0162-1.

[26] N. Chernov and C. Lesort, "Least squares fitting of circles," *J. Math. Imag. Vis.*, vol. 23, no. 3, pp. 239–252, 2005, doi: 10.1007/s10851-005-0482-8.

[27] G. Taubin, "Estimation of planar curves, surfaces, and nonplanar space curves defined by implicit equations with applications to edge and range image segmentation," *IEEE Trans. Pattern Anal. Mach. Intell.*, vol. 13, no. 11, pp. 1115–1138, Nov. 1991, doi: 10.1109/34.103273.

[28] F. Bukhari and M. N. Dailey, "Automatic radial distortion estimation from a single image," *J. Math. Imag. Vis.*, vol. 45, no. 1, pp. 31–45, 2013, doi: 10.1007/s10851-012-0342-2.

[29] T. Thormählen, H. Broszio, and I. Wassermann, "Robust line-based calibration of lens distortion from a single view," in *Proc. Mirage*, 2003, pp. 105–112.

[30] D. Gonzalez-Aguilera, J. Gomez-Lahoz, and P. Rodríguez-Gonzálvez, "An automatic approach for radial lens distortion correction from a single image," *IEEE Sensors J.*, vol. 11, no. 4, pp. 956–965, Apr. 2010, doi: 10.1109/jsen.2010.2076403.
[31] B. Benligiray and C. Topal, "Blind rectification of radial distortion by line straightness," in *Proc. 24th Eur. Signal Process. Conf. (EUSIPCO)*, Budapest, Hungary, Aug. 2016, pp. 938–942, doi: 10.1109/EUSIPCO.2016.7760386.
[32] M. Alemán-Flores, L. Alvarez, L. Gomez, and D. Santana-Cedrés, "Automatic lens distortion correction using one-parameter division models," *Image Process. Line*, vol. 4, pp. 327–343, Nov. 2014, doi: 10.5201/ipol.2014.106.
[33] D. Santana-Cedrés, L. Gomez, M. Alemán-Flores, A. Salgado, J. Esclarín, L. Mazorra, and L. Alvarez, "An iterative optimization algorithm for lens distortion correction using two-parameter models," *Image Process. Line*, vol. 6, pp. 326–364, Dec. 2016, doi: 10.5201/ipol.2016.130.
[34] M. Zhang, J. Yao, M. Xia, K. Li, Y. Zhang, and Y. Liu, "Line-based multi-label energy optimization for fisheye image rectification and calibration," in *Proc. IEEE Conf. Comput. Vis. Pattern Recognit. (CVPR)*, Jun. 2015, pp. 4137–4145, doi: 10.1109/CVPR.2015.7299041.
[35] D. Santana-Cedrés, L. Gomez, M. Alemán-Flores, A. Salgado, J. Esclarín, L. Mazorra, and L. Alvarez, "Estimation of the lens distortion model by minimizing a line reprojection error," *IEEE Sensors J.*, vol. 17, no. 9, pp. 2848–2855, May 2017, doi: 10.1109/JSEN.2017.2677475.
[36] Q. Y. Wang, Z. Y. Wang, and T. Smith, "Radial distortion correction in a vision system," *Appl. Opt.*, vol. 55, no. 31, pp. 8876–8883, 2016, doi: 10.1364/AO.55.008876.

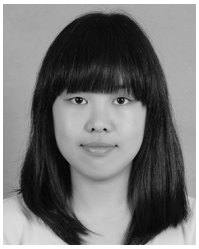

LUWEI ZHANG was born in 1988. She received the B.S. degree in measurement and control technology and instruments from the Changchun University of Science and Technology, Changchun, China, in 2011, and the M.S. degree in optical engineering from Zhejiang University, Hangzhou, China, in 2014. She is currently pursuing the Ph.D. degree in optical engineering with the University of Chinese Academy of Sciences, Beijing, China. Since 2017, she has been an Assistant Professor with the Changchun Institute of Optics, Fine Mechanics and Physics, Chinese Academy of Sciences. Her main research interests include optical design and computer vision.

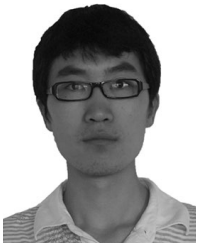

HONGBO SHANG was born in 1986. He received the B.S. degree in measurement and control technology and instruments from the Changchun University of Science and Technology, Changchun, China, in 2008, and the M.S. degree in optical engineering from Zhejiang University, Hangzhou, China, in 2011. He is currently pursuing the Ph.D. degree in optics with the University of Chinese Academy of Sciences, Beijing, China. Since 2013, he has been an Assistant Professor with the Changchun Institute of Optics, Fine Mechanics and Physics, Chinese Academy of Sciences. His main research interests include optical design and computer vision.

FANLU WU was born in 1988. He received the B.S. degree in measurement and control technology and instruments from the Changchun University of Science and Technology, Changchun, China, in 2011, the M.S. degree in astronomical techniques and methodology from the University of the Chinese Academy of Sciences, Beijing, China, in 2014, and the Ph.D. degree in instruments science and technology from Tianjin University, Tianjin, China, in 2018. Since 2018, he has been an Assistant Professor with the Changchun Institute of Optics, Fine Mechanics and Physics, Chinese Academy of Sciences. His research interests include computer vision, remote sensing, and planetary exploration.

RUI WANG was born in 1982. He received the B.S. degree in optical information science and technology from the Changchun University of Science and Technology, Changchun, China, in 2005, and the Ph.D. degree in optical engineering from the Graduate School of Chinese Academy of Sciences, Beijing, China, in 2010. Since 2012, he has been an Associate Professor with the Changchun Institute of Optics, Fine Mechanics and Physics, Chinese Academy of Sciences. His main research interests include optical design and laser active detection.

TAO SUN was born in 1980. He received the B.S. degree in information and computing sciences and the Ph.D. degree in computer software and theory from Jilin University, Changchun, China, in 2003 and 2010, respectively. Since 2012, he has been an Associate Professor with the Changchun Institute of Optics, Fine Mechanics and Physics, Chinese Academy of Sciences. His main research interests include image processing and automatic target recognition.

JINGJIANG XIE was born in 1954. He received the B.S. degree in optical instruments from the Changchun Institute of Optics and Fine Mechanics, Changchun, China, in 1982. Since 1997, he has been a Professor with the Changchun Institute of Optics, Fine Mechanics and Physics, Chinese Academy of Sciences. His main research interest includes advanced optical system design and manufacturing.